Chapter 6
Process-Based Simulation and Prediction of Plant Phenology Spatiotemporal Variations

Abstract Using tree first leaf unfolding and grass green-up data, and daily air temperature and precipitation data, local and regional unified phenology models were fitted and validated in northern China and the Inner Mongolian Grassland, respectively. Based on the regional phenology models, spatiotemporal patterns of first leaf unfolding dates and green-up dates were reconstructed over the continuous geographic coverage. Within the 250 optimum local first leaf unfolding models for the four tree species at 136 stations, the unified forcing and chilling models account for 83 and 17 %, respectively. Thus, forcing temperature predominantly influence first leaf unfolding dates in most parts of northern China, while the affect of chilling temperature was stronger for earlier than later first leaf unfolding species. Spatial and temporal validation confirmed the capability and reliability of the 16 regional unified species-specific models in predicting leaf unfolding dates in the four climate regions. The reconstructed leaf unfolding dates show a significant advancement in most parts of northern China over 1960–2009, which is stronger for earlier than later first leaf unfolding species. For grass green-up modeling, previous temperature accumulation controls green-up dates of the three grass species at three stations, while both previous temperature and precipitation accumulations control green-up dates of these grass species at another three stations. The accumulated precipitation plays a more important role as the precondition of forcing temperature than as the supplementary condition of forcing temperature in triggering green-up of grasses. The accuracy of the regional unified models in simulating and predicting green-up dates of grasses at internal and external stations is at acceptable levels overall. The reconstructed mean green-up dates for the three grass species represented a similar spatial pattern across the Inner Mongolian Grassland, which is aligned approximately along the thermal and moisture gradient. Spatial patterns of green-up date linear trends indicate a significant advancement at 40.3–71.4 % of all grids over the Inner Mongolian Grassland during 1983–2009.

Keywords *UniForc* model · *UniChill* model · Traditional thermal time model · Air temperature-precipitation parallel model · Air temperature-precipitation sequential model · Regional unified model · Spatiotemporal patterns

X. Chen, *Spatiotemporal Processes of Plant Phenology*,
SpringerBriefs in Geography, DOI 10.1007/978-3-662-49839-2_6

6.1 Introduction

Statistical phenology models are probabilistic and based on statistical hypotheses. Parameters of statistical models are estimated from empirical data using various statistical fitting methods (Chuine et al. 2003). Because these models may not consider biological processes, they can only fit the specific sample dataset of a given phenological occurrence date by means of climatic factors, but normally cannot be used to extrapolate and predict the phenological occurrence date beyond the time period of model fitting. By contrast, mechanistic (or process-based) phenology models are causal and based on physiological and ecological hypotheses. The known or assumed cause-effect relationships between biological processes and driving factors in the plant's environment should be included in a mechanistic model only if information on its impacts on the process is available. Although parameters of mechanistic models have physical dimensions that can theoretically be measured directly instead of being estimated by fitting, this is rarely possible in the practice (Chuine et al. 2003). Generally speaking, this type of phenology models may not only simulate the specific sample dataset of a given phenological occurrence date by means of climatic factors but also predict phenological occurrence dates beyond the time period of model fitting.

So far, most of mechanistic phenology models have been created for fitting and predicting spring phenology of individual trees at station scales, such as budburst, leaf unfolding and flowering dates (Landsberg 1974; Cannell and Smith 1983; Murray et al. 1989; Hänninen 1990; Kramer 1994a; Chuine et al. 1998; Linkosalo et al. 2008; Morin et al. 2009; Fu et al. 2012; Xu and Chen 2013). The basic hypothesis of local species-specific phenology models is that spring tree phenology is triggered mainly by chilling temperatures during the previous autumn and winter, and forcing temperatures during the current spring (Chuine 2000). The simplest models are only based on the accumulation of forcing temperatures that induce plant growth and reproduction after bud dormancy has been broken in spring (Cannell and Smith 1983; Hunter and Lechowicz 1992; Chuine et al. 1999). More sophisticated models are based on the accumulation of both chilling temperatures and forcing temperatures. Because chilling temperatures may influence bud dormancy and accelerate bud growth from the state of quiescence to the state of budburst, the negative relationship between the state of forcing and the state of chilling has been considered in these models, namely, the less chilling temperatures are received, the more forcing temperatures are subsequently needed to trigger budburst (Cannell and Smith 1983; Murray et al. 1989; Kramer 1994b; Chuine 2000).

Applications of these spring phenology models have been restricted to the relevant phenological event occurrence date at given locations (Chuine et al. 1998, 1999). However, as plant phenology has found a renewal in the context of global climate change, there is an urgent need for simulating and predicting phenological event occurrence dates at regional scales (Chuine et al. 2000). For meeting the needs, regional unified species-specific models should be developed by upscaling species-specific phenology models from individual stations to a region. A regional

unified species-specific model assumes that responses of a phenological event occurrence date to temperature at various stations are not significantly different within the same climate region (Xu and Chen 2013).

Moreover, most phenology models were developed for tree species, rather than non-woody species (Chuine et al. 2003). In comparison with forests, grasslands are one of the most widespread vegetation types worldwide, and play a major but poorly defined role in the global carbon cycle and climate change. As seasonal distribution of rainfall is a major determinant of plant development and production in many semiarid and arid regions (Hall et al. 2000), the moisture factors should be taken into account in the grass phenology models. Thus, how to couple seasonal precipitation to temperature-based models is the key difficulty. Unfortunately, there is no a consistent pattern of seasonal precipitation impacts on grass phenology over different grassland ecosystems (Cleland et al. 2006; Sherry et al. 2007; Shinoda et al. 2007; Jentsch et al. 2009; Crimmins et al. 2010, 2011; Lesica and Kittelson 2010). Examining the combined effects of air temperature and precipitation during late winter and early spring on green-up date of the dominant grass species by means of process-based models is crucial not only for revealing ecological mechanisms of grassland phenology, but also for predicting appropriate grazing and harvesting times, as well as estimating net primary productivity and carbon sequestration in grassland ecosystems (Chen et al. 2014).

6.2 Leaf Unfolding Simulation and Prediction Across Northern China

6.2.1 Study Area and Tree Species

The study area is located in northern China's temperate zone, which includes cold temperate, humid/sub-humid middle temperate, humid/sub-humid warm temperate, semi-arid middle/warm temperate, and arid middle/warm temperate regions (Fig. 6.1, China Meteorological Administration 1978). As no phenological stations are located in the cold temperate region, only four climate regions were involved.

Salix matsudana, *Populus simonii*, *Ulmus pumila* and *Prunus armeniaca* were chosen as indicator plant species because they are all native deciduous trees and grow broadly in the study area. To reconstruct phenological time series for the four tree species at grid scales, their possible distribution areas were determined according to species distribution altitude limits and desert boundaries.

6.2.2 Phenological and Climate Data

The first leaf unfolding data for *Salix matsudana*, *Populus simonii*, *Ulmus pumila* and *Prunus armeniaca* were acquired from the China Meteorological Administration

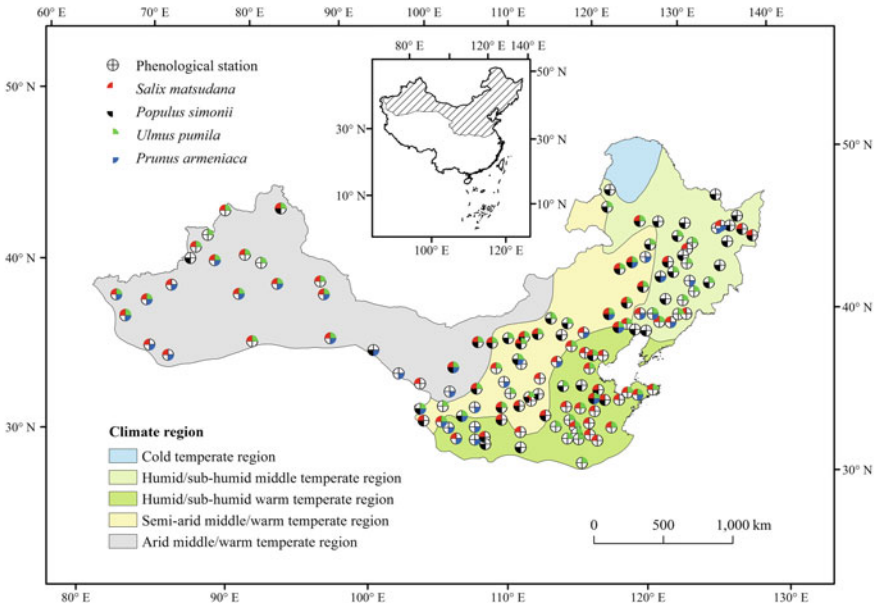

Fig. 6.1 Location of phenological stations with the four tree species observations in different climate regions [Reprinted from Xu and Chen (2013), with permission from John Wiley and Sons]

(Chen 2009). Altogether, 136 stations (with phenological time series of more than 10 years from 1981 to 2005) were selected for first leaf unfolding modeling. The number of stations is different for the four tree species, namely, 77 stations for *Salix matsudana*, 61 stations for *Populus simonii*, 72 stations for *Ulmus pumila*, and 40 stations for *Prunus armeniaca* (Fig. 6.1).

Climate data were obtained from the China Meteorological Data Sharing Service System (http://cdc.cma.gov.cn/), including daily mean air temperature at 343 meteorological stations in the northern China's temperate zone over the 1959-2009 period. For reconstructing spatiotemporal patterns of first leaf unfolding dates at grid scales, daily mean air temperatures were interpolated into 8 km × 8 km grids over the study area using ANUSPLIN 4.2 (Hutchinson 2002) and Digital Elevation Model (DEM) data derived from the United States Geological Survey. Meanwhile, gridded daily mean air temperature data at a few phenological stations without meteorological observations were also produced and used.

6.2.3 Phenology Models

The *UniForc* and *UniChill* models (Chuine 2000) were employed to fit first leaf unfolding time series of the four tree species at each station from 1981 to 2005. The *UniForc* model considers only the effect of forcing temperatures during spring. The

assumption is that first leaf unfolding appears when the state of forcing, S_f, reaches a critical value F^* on the date of y (Eq. 6.1):

$$S_f = \sum_{t_1}^{y} R_f(x_t) = F^* \tag{6.1}$$

The state of forcing is defined as a daily accumulation of the rate of forcing, $R_f(x_t)$, which begins at t_1 (day of year, DOY). The rate of forcing is an exponential function and x_t is the daily mean air temperature (Eq. 6.2):

$$R_f(x_t) = \frac{1}{1 + e^{d(x_t - e)}} \tag{6.2}$$

The *UniForc* model includes four parameters where t_1 is usually set on 1 January and d, e and F^* were fitted, with $d < 0$ and $e > 0$.

The *UniChill* model considers the effect of both chilling temperatures during the dormancy period and forcing temperatures during the growth period. The hypothesis is that dormancy breaks when the state of chilling, S_c, reaches a critical value C^* on the date of t_1 (Eq. 6.3):

$$S_c = \sum_{t_0}^{t_1} R_c(x_t) = C^* \tag{6.3}$$

The state of chilling is defined as a daily accumulation of the rate of chilling, $R_c(x_t)$, which begins at t_0 (DOY). The rate of chilling is also an exponential function and x_t is the daily mean air temperature (Eq. 6.4):

$$R_c(x_t) = \frac{1}{1 + e^{a(x_t - c)^2 + b(x_t - c)}} \tag{6.4}$$

On the date of t_1, forcing units start to accumulate until it reaches a critical value F^* (Eqs. 6.1 and 6.2). The *UniChill* model contains seven fitted parameters, in which a, b, c, C^* pertain to the chilling function and d, e, F^*, belong to the forcing function. t_0 is commonly fixed on 1 September of the preceding year.

The species-specific parameters of *UniForc* and *UniChill* models at a station were determined by the lowest value of the root mean square error (RMSE, Eq. 6.5), while the optimum local model (*UniForc* or *UniChill*) was selected by the lowest value of the Akaike Information Criterion (AIC, Eq. 6.6) (Akaike 1973). In addition, the Nash–Sutcliffe Efficiency index (NSE, Eq. 6.7) (Nash and Sutcliffe 1970) was used to assess the reliability of model validation in the spatial extrapolation in comparison with the null model (mean dates of first leaf unfolding). A negative NSE value denotes that the model performs worse than the null model, whereas a positive NSE value (with a maximum value of 1) indicates that the model

explains more variance than the null model. Moreover, the closer the NSE value to 1, the higher the model reliability, while the closer the NES value to 0, the lower the model reliability.

$$\mathrm{RMSE} = \sqrt{\frac{\sum_{i=1}^{n} (obs_i - pre_i)^2}{n}} \tag{6.5}$$

$$\mathrm{AIC} = n \times \ln\left(\frac{\sum_{i=1}^{n} (obs_i - pre_i)^2}{n}\right) + 2(k+1) \tag{6.6}$$

$$\mathrm{NSE} = 1 - \frac{\sum_{i=1}^{n} (obs_i - pre_i)^2}{\sum_{i=1}^{n} \left(obs_i - \overline{obs}\right)^2} \tag{6.7}$$

where obs_i is the observed value in year i; pre_i is the simulated (or predicted) value in year i; $\overline{obs}$ is mean observed value in the validation period; n is the number of years; k is the number of parameters (Xu and Chen 2013).

6.2.4 Local First Leaf Unfolding Modeling

Within the selected 250 optimum models for the four tree species at 136 stations, the *UniForc* model accounts for 83 % (207 models), which implies that forcing temperature predominantly influence first leaf unfolding date of the four tree species in most parts of northern China's temperate zone. For the rest 43 optimum models (17 % of total) in the form of *UniChill*, the number and percentage of stations with effective chilling temperature steadily decreases from earlier first leaf unfolding tree species (such as *Salix matsudana* and *Populus simonii*) to later first leaf unfolding tree species (such as *Ulmus pumila* and *Prunus armeniaca*), namely, 18 stations (23 % of 77) for *Salix matsudana*, 13 stations (21 % of 61) for *Populus simonii*, 11 stations (15 % of 72) for *Ulmus pumila* and 1 station (3 % of 40) for *Prunus armeniaca*. This indicates that the influence of chilling temperature on first leaf unfolding date was stronger for earlier first leaf unfolding species than later first leaf unfolding species in northern China. The RMSEs for differences between observed and simulated first leaf unfolding dates range from 0.7 days to 10.2 days for the 250 optimum models, and the mean RMSE is 3.7 days (Xu and Chen 2013).

6.2.5 Regional Unified First Leaf Unfolding Modeling

Regional unified models were selected from optimum local species-specific models based on their capability in the spatial extrapolation. For achieving this goal, each

optimum local species-specific model was employed to extrapolate first leaf unfolding dates of corresponding species at all other stations within its located climate region during 1981–2005. The extrapolation errors were evaluated by NES and RMSE, and the best local species-specific model with effective extrapolation (NSE > 0) and the lowest value of the RMSE was determined as the regional unified model for each species and each climate region (Table 6.1). Within the 16 regional unified models, only the model for *Salix matsudana* first leaf unfolding in the humid/sub-humid middle temperate region contains both chilling and forcing temperature accumulations (*UniChill* model), while the other 15 models require only forcing temperature accumulation (*UniForc* model). The mean RMSE of each regional unified model at stations with effective extrapolation ranges from 3.3 to 6.0 days (Table 6.1).

The temporal validation of the 16 regional unified models in years beyond the time period of model fitting shows that the observed first leaf unfolding date correlates significant positively ($P < 0.01$) with the predicted first leaf unfolding date

Table 6.1 Regional unified models and their assessments in spatial extrapolation over 1981–2005 for the four tree species in the four climate regions (Xu and Chen 2013)

Species	Climate region	Number of stations	Regional unified models	Number of stations with NSE > 0	Percentage (%)	Mean RMSE*
Salix matsudana	HSMT	10	*UniChill*	8	80	5.44
	HSWT	25	*UniForc*	16	64	6.01
	SMWT	22	*UniForc*	12	55	5.79
	AMWT	20	*UniForc*	14	70	3.57
Populus simonii	HSMT	19	*UniForc*	12	63	4.45
	HSWT	13	*UniForc*	11	85	5.80
	SMWT	24	*UniForc*	17	71	4.33
	AMWT	5	*UniForc*	3	60	3.43
Ulmus pumila	HSMT	11	*UniForc*	9	82	5.97
	HSWT	19	*UniForc*	14	74	5.70
	SMWT	24	*UniForc*	14	58	5.17
	AMWT	18	*UniForc*	8	44	4.95
Prunus armeniaca	HSMT	7	*UniForc*	7	100	4.94
	HSWT	8	*UniForc*	6	75	4.91
	SMWT	10	*UniForc*	6	60	3.80
	AMWT	15	*UniForc*	10	67	3.32

HSMT humid/sub-humid middle temperate region, *HSWT* humid/sub-humid warm temperate region, *SMWT* semi-arid middle/warm temperate region, *AMWT* arid middle/warm temperate region

*Mean RMSE at stations with NSE > 0

during 2006–2009 in 15 of 16 models. The RMSE of each regional unified model in the temporal validation ranges from 2.0 and 10.6 days (Fig. 6.2). As the mean RMSEs of temporal validation for each tree species in the four climate regions (Fig. 6.2) are only slightly larger (0.4–1.6 days) than those of spatial validation for each tree species in the four climate regions (Table 6.1), the process-based regional unified models provide a robust tool for predicting first leaf unfolding dates of the four tree species in northern China's temperate zone.

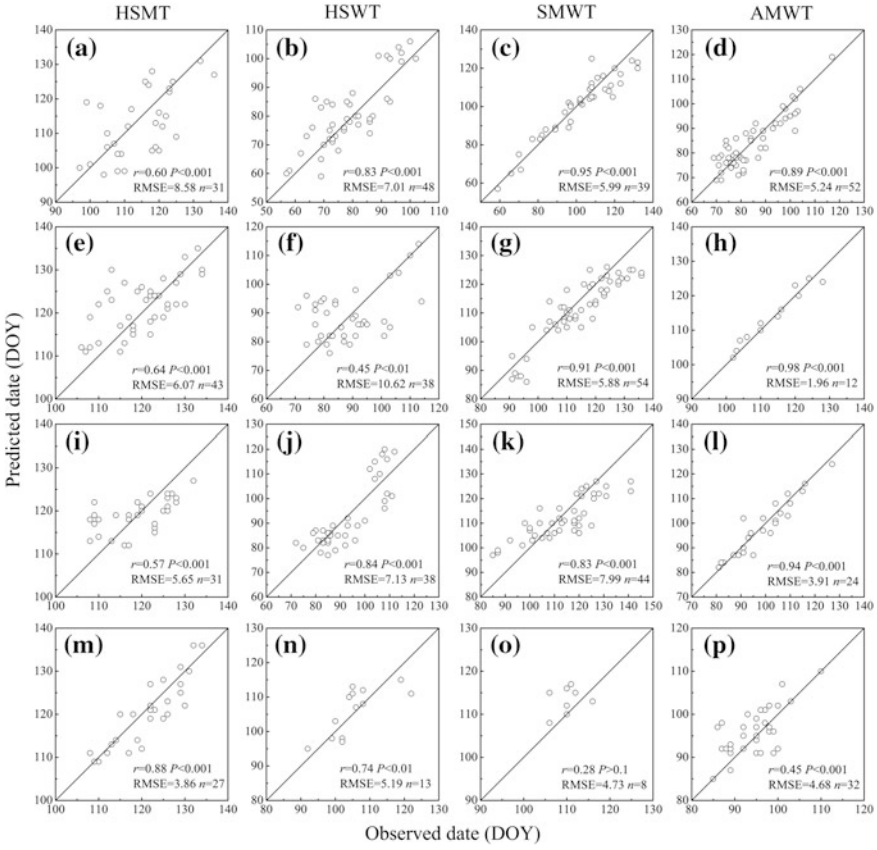

Fig. 6.2 Comparison between observed first leaf unfolding date and predicted first leaf unfolding date based on regional unified species-specific models in the four climate regions during 2006–2009. **a–d** *Salix matsudana*, **e–h** *Populus simonii*, **i–l** *Ulmus pumila*, **m–p** *Prunus armeniaca* [Reprinted from Xu and Chen (2013), with permission from John Wiley and Sons]

6.2.6 *Spatiotemporal Patterns of First Leaf Unfolding Dates*

Based on the 16 regional unified species-specific models, long-term first leaf unfolding dates for the four tree species across northern China have been reconstructed using gridded daily mean temperature data from 1959 to 2009. At the grid level, a significantly advancing trend in first leaf unfolding dates was detected in most parts of the possible distribution area of each tree species over 1960–2009. It should be noted that the spatial differentiation in linear trends of first leaf unfolding dates decreases gradually from the earlier to the later first leaf unfolding species (Fig. 6.3).

At the climate region level, first leaf unfolding dates of the four tree species display a synchronously significant advancement ($P < 0.001$) from 1960 to 2009 with trend values ranging from −1.2 days per decade to −2.2 days per decade (Fig. 6.4).

Across northern China's temperate zone, regional mean first leaf unfolding dates advanced significantly ($P < 0.001$) at a slowing rate from earlier first leaf unfolding species to later first leaf unfolding species, namely, –1.61 days per decade for *Salix matsudana*, –1.59 days per decade for *Populus simonii*, –1.41 days per decade for *Ulmus pumila*, and –1.39 days per decade for *Prunus armeniaca* during 1960–2009.

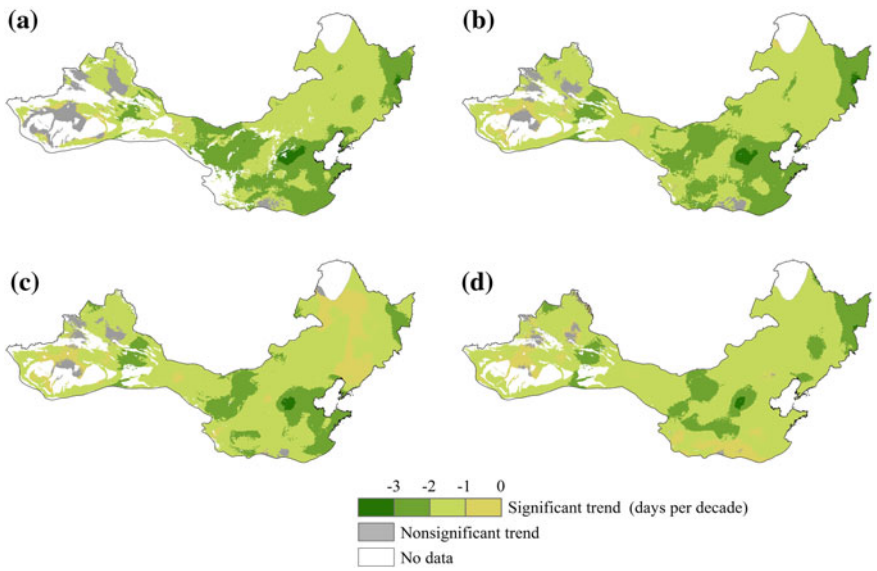

Fig. 6.3 Spatial pattern of linear trends in first leaf unfolding dates in northern China's temperate zone over 1960–2009. **a** *Salix matsudana*, **b** *Populus simonii*, **c** *Ulmus pumila*, **d** *Prunus armeniaca* [Reprinted from Xu and Chen (2013), with permission from John Wiley and Sons]

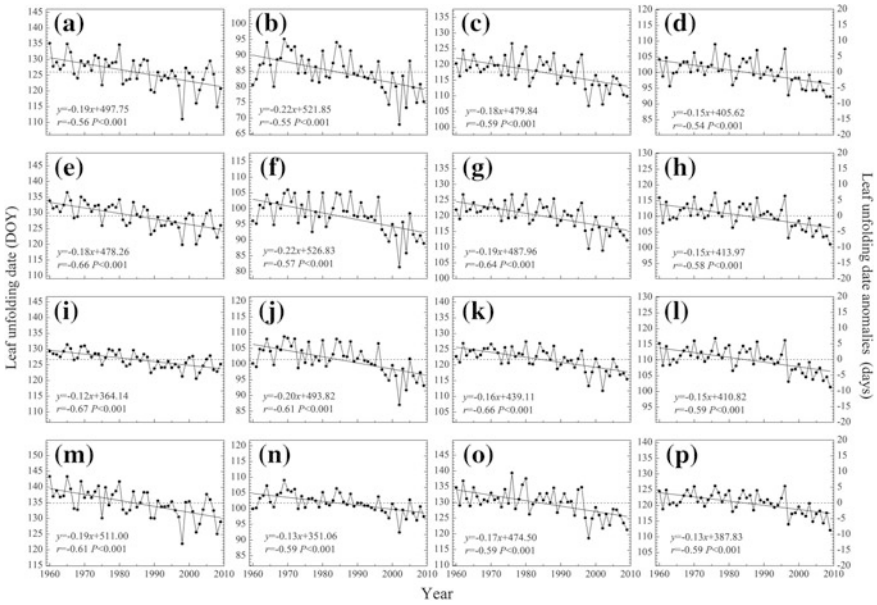

Fig. 6.4 Linear trends in first leaf unfolding dates of the four tree species in the humid/subhumid middle temperate region (HSMT, first column), humid/subhumid warm temperate region (HSWT, second column), semiarid middle/warm temperate region (SMWT, third column), and arid middle/warm temperate region (AMWT, fourth column) over 1960–2009. **a–d** *Salix matsudana*, **e–h** *Populus simonii*, **i–l** *Ulmus pumila*, **m–p** *Prunus armeniaca* [Reprinted from Xu and Chen (2013), with permission from John Wiley and Sons]

6.3 Green-up Simulation and Prediction in the Inner Mongolian Grassland

6.3.1 Study Area and Grass Species

The Inner Mongolia Autonomous Region is located in temperate northern China (Fig. 6.5). Influenced by both East Asian monsoon along the east coast and inland drought in the west, the climate can be divided into temperate subhumid, semiarid and arid regions from east to west (China Meteorological Administration 1978). The topographical structure is composed of the Inner Mongolian Plateaus with an average height of 1000 m above sea level and the surrounding catenulate mountains at 1000–2500 m above sea level. The annual mean air temperature increases from −5 °C in the northeast to 10 °C in the southwest, while the annual mean total precipitation decreases from 530 mm in the east to 35 mm in the west. Along with the thermal-moisture gradient, the vegetation contains six belts from northeast to southwest, namely, coniferous forest, deciduous broadleaf forest, forest steppe,

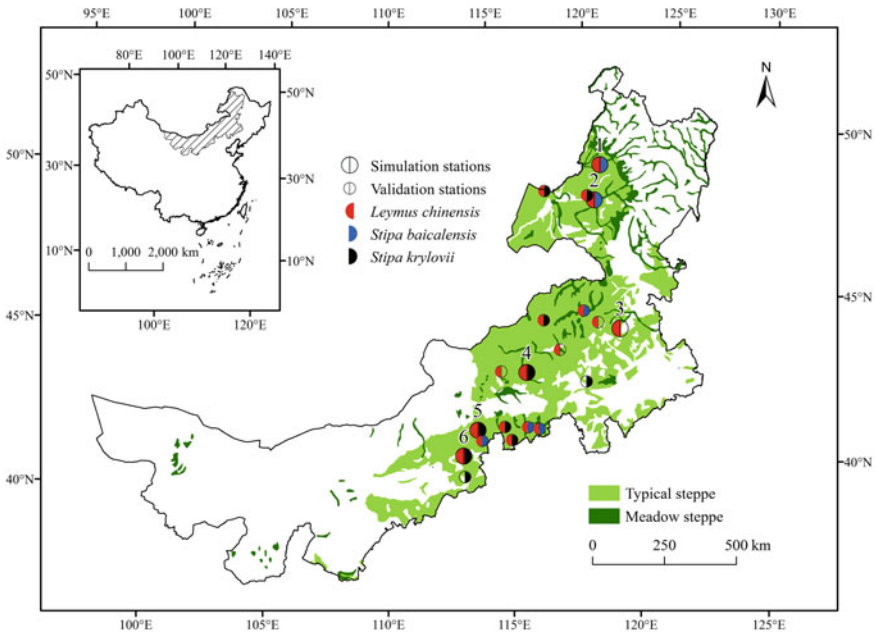

Fig. 6.5 Location of phenological stations with the three dominant grass species observations in the Inner Mongolian Grassland

typical steppe, desert steppe, and desert (Editorial Board of the Inner Mongolian Grassland 1991). In addition, some intrazonal vegetation types are distributed across lowland, sand plain and mountainous areas, such as meadow steppe and subshrubs. Because typical steppe and meadow steppe are characterized by good nutritional quality, high productivity, mowing suitability, and strong palatability, they are the most important pasture in the temperate zone of China. Six grassland meteorological experiment stations were selected for process-based modeling, in which E'ergunayouqi, Ewenkeqi and Bayartuhushuo are located in the meadow steppe areas, while Xilinhot, Xianghuangqi and Chaharyouyihouqi lie in the typical steppe areas (Fig. 6.5). Geo-location parameters and thermal-moisture conditions of the six stations are listed in Table 6.2. At these stations, three dominant grass species in the Inner Mongolian Grassland (*Leymus chinensis*, *Stipa baicalensis* and *Stipa krylovii*) were chosen as indicator species for process-based modeling.

6.3.2 Phenological and Climate Data

The phenological data include green-up dates of the three grass species at six grassland meteorological experiment stations from 1983 to 2009 and at 14 ecological stations from 2005 to 2009. The phenological observation was carried out in

Table 6.2 Geo-location parameters and thermal-moisture conditions at each station (Chen et al. 2014)

Station	Number[a]	North latitude	East longitude	Elevation (m a.s.l)	Annual mean temperature (°C)	Annual precipitation (mm)
E'ergunayouqi	1	50°15′	121°11′	582	−2.0	375.9
Ewenkeqi	2	49°09′	119°45′	621	−1.0	344.9
Bayartuhushuo	3	45°04′	120°20′	629	3.8	438.9
Xilinhot	4	43°57′	116°04′	991	3.0	269.9
Xianghuangqi	5	42°14′	113°50′	1323	3.9	272.0
Chaharyouyihouqi	6	41°27′	113°11′	1425	4.2	325.7

[a] The station number is the same as in Fig. 6.5

natural pastures with an area of 10000 m^2 at each station. The green-up of a grass species is identified when 10 % of individual grasses display green leaves and grow up to one centimeter in spring or early summer (China Meteorological Administration 1993; Study Group of Animal Husbandry Climate Regionalization for China's Pastoral Areas 1988). As different species have different distribution ranges, observed green-up data of the three grass species are not identical at each station. Namely, *Leymus chinensis* has been observed at the six grassland meteorological experiment stations in both typical and meadow steppe areas, while *Stipa baicalensis* and *Stipa krylovii* have been observed at E'ergunayouqi and Ewenkeqi in meadow steppe areas, and at Xilinhot, Xianghuangqi and Chaharyouyihouqi in typical steppe areas, respectively (Fig. 6.5).

Statistical analysis shows that mean green-up dates of *Leymus chinensis* occurred during 17 April to 6 May with standard deviations (SD) between 4.5 and 6.9 days over the six stations, while mean green-up dates of *Stipa baicalensis* and *Stipa krylovii* appeared during 1 May to 7 May with a SD of 5.0 days at E'ergunayouqi and Ewenkeqi, and during 15 April to 28 April with SDs between 4.5 and 7.1 days at Xilinhot, Xianghuangqi and Chaharyouyihouqi, respectively. A significant advancement in green-up date ($P < 0.01$–0.001) was detected at Chaharyouyihouqi for *Leymus chinensis* and *Stipa krylovii* from 1983 to 2009, while a significant delay ($P < 0.05$) was found at Xilinhot for *Stipa krylovii* (Table 6.3).

Daily mean air temperature and daily precipitation data at 118 meteorological stations during 1983–2009 were collected for green-up modelling. In order to reconstruct time series of grass green-up dates over a continuous geographic coverage, the climate data interpolation package ANUSPLIN 4.2 (Hutchinson 2002) and Digital Elevation Model (DEM) data derived from the US Geological Survey were used to interpolate the daily mean air temperature and daily precipitation into 8 km × 8 km grids over the Inner Mongolia Autonomous Region.

Table 6.3 Statistical characteristic values of green-up dates of the three grass species at each station during 1983–2009 (Chen et al. 2014)

Station number[a]	Species	Number of years	Mean date (day of year)	Standard deviation (days)	Linear trends (days per decade)
1	*L. chinensis*	22	126	4.5	1.98
	S. baicalensis	24	127	5.0	–0.63
2	*L. chinensis*	21	120	4.5	0.30
	S. baicalensis	19	121	5.0	1.35
3	*L. chinensis*	16	112	4.9	–1.83
4	*L. chinensis*	17	109	5.1	–1.23
	S. krylovii	21	105	6.5	4.85*
5	*L. chinensis*	23	107	5.0	–0.09
	S. krylovii	23	106	4.5	1.69
6	*L. chinensis*	24	118	6.9	–5.45***
	S. krylovii	24	118	7.1	–4.63**

*$P < 0.05$, ** $P < 0.01$, *** $P < 0.001$

[a]The station number is the same as in Fig. 6.5

6.3.3 Phenology Models

To examine the combined effects of air temperature and precipitation on green-up date of the dominant grass species, traditional thermal time model and two revised thermal time models coupling air temperature and precipitation were employed to fit green-up dates of *Leymus chinensis*, *Stipa baicalensis* and *Stipa krylovii*.

The traditional thermal time model considers only the effect of forcing air temperatures during spring. The hypothesis is that green-up appears when the state of forcing, S_T, reaches a critical value F^* on the date of y (Eq. 6.8):

$$S_T = \sum_{t_0}^{y} R_T(T_t) = F^* \tag{6.8}$$

The state of forcing is defined as a daily accumulation of the rate of forcing above a base air temperature T_b, $R_T(T_t)$, which starts at t_0 (DOY) and T_t is the daily mean air temperature. The rate of forcing in the traditional thermal time model is defined by Eq. 6.9:

$$R_T(T_t) = \begin{cases} 0 & T_t \leq T_b \\ T_t - T_b & T_t > T_b \end{cases} \tag{6.9}$$

This model contains three parameters where the starting date of the temperature accumulation (t_0) was fixed on 1 January, and the base temperature (T_b) and the critical value of state of forcing (F^*) were fitted.

The revised thermal time model considers the effects of both forcing air temperatures and precipitations from 1 January to green-up date. According to the field observations during 2004–2006 in Ewenkeqi, accumulated late winter and early spring precipitation, usually falling as snow, is at least as important as spring temperature in triggering green-up of grass species (Chen et al. 2008). A statistical analysis in the Mongolian Grasslands has also shown that precipitation or snow melt events in spring could trigger grass to start growing (Shinoda et al. 2007). One possible explanation for this association is that grass roots cannot start to grow until the ground has been warmed and humidified above 0 °C, after snow melt. Namely, more snow fall during late winter and early spring can mean more soil moisture storage as spring temperature increases, and induce earlier green-up, whereas less snow fall during late winter and early spring can create a soil moisture shortage coupling with rapid spring temperature increases, and force later green-up. The revised thermal time model assumes therefore that green-up of grasses is triggered by accumulated spring air temperature and accumulated late winter and early spring precipitation in the form of snow. This model contains two approaches.

The air temperature-precipitation parallel model assumes that accumulated air temperature and precipitation are equivalently important in triggering green-up of grasses. That is, green-up occurs when the state of forcing air temperature, S_T and the state of forcing precipitation, S_P, achieve critical values F^* and P^*on the date of y (Eqs. 6.8 and 6.10):

$$S_P = \sum_{t_0}^{y} R_P(P_t) = P^* \tag{6.10}$$

The state of precipitation is defined as a daily accumulation of the rate of precipitation, R_p (P_t), which starts at t_0 (DOY) and P_t is the daily precipitation (mm). Here, the starting date of precipitation accumulation was also set as 1 January (t_0). The rate of precipitation in the air temperature-precipitation parallel model is defined by Eq. 6.11:

$$R_P(P_t) = P_t \tag{6.11}$$

There are three fitted parameters in the air temperature-precipitation parallel model, namely, T_b, F^* and P^*.

The air temperature-precipitation sequential model assumes that air temperature and precipitation trigger green-up of grasses sequentially, namely, the effect of

forcing air temperature on green-up occurs when the state of forcing precipitation, S_P, achieves critical value P^*on the date of t_1 (Eq. 6.12):

$$S_P = \sum_{t_0}^{t_1} R_P(P_t) = P^* \tag{6.12}$$

The state of precipitation is defined as a daily accumulation of the rate of precipitation, R_p (P_t), which starts at t_0 (DOY) and terminates at t_1 (DOY). The rate of precipitation in the air temperature-precipitation sequential model is also defined by Eq. 6.11. The time point t_1 represents not only the end date of precipitation accumulation but also the starting date of temperature accumulation. The air temperature-precipitation sequential model contains also three fitted parameters T_b, $F^*$and P^*. Because grass green-up appeared after the date daily mean air temperature rose above 0 °C and before the date daily mean air temperature surpassed 5 °C (Study Group of Animal Husbandry Climate Regionalization for China's Pastoral Areas 1988), a candidate range of T_b was set between daily mean air temperatures of 0 and 5 °C (Chen et al. 2014).

The species-specific parameters of the traditional thermal time model and the revised thermal time models coupling air temperature and precipitation were determined by the lowest value of the RMSE (Eq. 6.5), while the optimum local model (traditional thermal time model or one of the revised thermal time models coupling air temperature and precipitation) was selected by the lowest value of AIC (Eq. 6.6).

To assess performances of the regional unified models in spatial extrapolation, these models were validated by predicting green-up dates of the three grass species from 2005 to 2009 at the 14 external stations within the research region (Fig. 6.5). The precision of the spatial validation was evaluated by correlation coefficient and RMSE between observed and predicted green-up dates.

6.3.4 Local Green-up Modeling

Within the 11 optimum models for the three grass species at six stations, six models belong to the traditional thermal time model. They were created at E'ergunayouqi, Ewenkeqi and Chaharyouyihouqi (Table 6.4). This indicates that late winter and early spring precipitation did not significantly influence green-up dates of the three grass species at these three locations. The RMSEs for *Leymus chinensis* green-up modeling ranged from 3.6 to 5.8 days, whereas the RMSEs for *Stipa baicalensis* and *Stipa krylovii* green-up modeling were between 4.0 and 5.6 days. Moreover, the traditional thermal time model can explain 48 % (R^2, $P < 0.001$) and 47 % ($P < 0.001$) of the observed interannual variations in *Leymus chinensis* and *Stipa baicalensis* green-up dates at Ewenkeqi, and 57 % ($P < 0.001$) and 40 %

($P < 0.001$) of the observed interannual variations in *Leymus chinensis* and *Stipa krylovii* green-up dates at Chaharyouyihouqi, respectively. In contrast, coefficients of determination (R^2) between observed and predicted *Leymus chinensis* green-up dates and between observed and predicted *Stipa baicalensis* green-up dates are only 4 and 14 % ($P > 0.05$), respectively at E'ergunayouqi, which implies that the traditional thermal time model cannot effectively explain the observed interannual variations in *Leymus chinensis* and *Stipa baicalensis* green-up dates there (Table 6.4).

The green-up dates of *Leymus chinensis* and *Stipa krylovii* at Bayartuhushuo, Xilinhot and Xianghuangqi were best fitted by the revised thermal time models coupling air temperature and precipitation, including four air temperature-precipitation sequential models and one air temperature-precipitation parallel model. The RMSEs for *Leymus chinensis* green-up modeling ranged from 3.1 to 6 days over the three stations, whereas the RMSEs for *Stipa krylovii* green-up modeling were 6.3 days at both Xilinhot and Xianghuangqi. Thus, accumulated late winter and early spring precipitation might be the precondition (sequential model) or supplementary condition (parallel model) of the dominant effect of forcing temperature in triggering green-up of grass species at these three locations. Coefficients of determination (R^2) show that the optimum revised thermal time models can explain 68 % ($P < 0.001$) of the observed interannual variation in *Leymus chinensis* green-up date at Bayartuhushuo, and 63 % ($P < 0.001$) and 23 % ($P < 0.05$) of the observed interannual variations in *Leymus chinensis* and *Stipa*

Table 6.4 Parameters and simulation accuracies of optimum local species-specific models (Chen et al. 2014)

Station number	Species	Optimum model[a]	T_b (°C)	F^* (°C)	P^* (mm)	R^2	RMSE (days)
1	*L. chinensis*	M_t	0.0	119.1	–	0.04	5.8
	S. baicalensis	M_t	0.2	135.3	–	0.14	5.2
2	*L. chinensis*	M_t	0.0	105.8	–	0.48^{***}	3.6
	S. baicalensis	M_t	0.1	117.9	–	0.47^{***}	4.0
3	*L. chinensis*	$M_{t\text{-}p2}$	0.2	97.0	2.0	0.68^{***}	3.1
4	*L. chinensis*	$M_{t\text{-}p1}$	2.5	42.5	5.9	0.63^{***}	3.6
	S. krylovii	$M_{t\text{-}p2}$	0.1	52.6	5.1	0.23^{*}	6.3
5	*L. chinensis*	$M_{t\text{-}p2}$	0.0	105.1	2.5	0.07	6.0
	S. krylovii	$M_{t\text{-}p2}$	0.1	89.8	3.0	0.01	6.3
6	*L. chinensis*	M_t	0.0	185.6	–	0.57^{***}	4.5
	S. krylovii	M_t	0.2	170.1	–	0.40^{***}	5.6

[a]M_t traditional thermal time model, $M_{t\text{-}p1}$ air temperature-precipitation parallel model, $M_{t\text{-}p2}$ air temperature-precipitation sequential model

$^*P < 0.05$, $^{**}P < 0.01$, $^{***}P < 0.001$

krylovii green-up dates at Xilinhot. However, R^2 values between observed and predicted *Leymus chinensis* green-up dates and between observed and predicted *Stipa krylovii* green-up dates are only 7 and 1 % ($P > 0.05$), respectively at Xianghuangqi, which means that the air temperature-precipitation sequential model cannot effectively explain the observed interannual variation in *Leymus chinensis* and *Stipa krylovii* green-up dates at that location (Table 6.4).

Overall, parameter estimates of the optimum local species-specific models show that T_b and F^* ranged from 0 to 2.5 °C and from 42.5 to 185.6 °C, respectively, while P^* ranged from 2 to 5.9 mm (Table 6.4). As F^* values of the traditional thermal time model are generally larger than those of the air temperature-precipitation parallel and sequential models, precipitation has compensation effects to air temperature in triggering green-up of grass species. Simulation errors for the 11 optimum local species-specific models, as measured by RMSE are between 3.1 and 6.3 days, and the mean RMSE is 4.9 days.

6.3.5 Regional Unified Green-Up Modeling

The basic hypothesis for regional green-up modeling is that local model estimates of green-up response to climatic factors for a grass species are not significantly different within its distribution range, based on which regional models can be constructed by pooling time series of species-specific green-up dates from different sample stations (García-Mozo et al. 2008; Delpierre et al. 2009). For *Leymus chinensis* green-up modeling, time series of green-up dates from all six sample stations within the research region were combined. For *Stipa baicalensis* and *Stipa krylovii* green-up modeling however, time series of green-up dates from E'ergunayouqi and Ewenkeqi within meadow steppe areas, and from Xilinhot, Xianghuangqi and Chaharyouyihouqi within typical steppe areas were merged, respectively. Results show that the traditional thermal time model has higher simulation parsimony and efficiency than the revised thermal time models coupling air temperature and precipitation for *Stipa baicalensis*. By contrast, the revised thermal time models coupling air temperature and precipitation has higher simulation parsimony and efficiency than the traditional thermal time model for *Leymus chinensis* (air temperature-precipitation parallel model) and *Stipa krylovii* (air temperature-precipitation sequential model). Simulation errors for the three optimum regional species-specific models, as measured by RMSE range from 5 to 9.2 days (Table 6.5), and the mean RMSE is 7 days.

To validate performances of the three regional models in spatial extrapolation, daily mean air temperature and daily precipitation data at the 14 external stations during 2005–2009 were substituted into regional species-specific models and the predicted green-up dates were compared with field observations. As sample sizes of

Table 6.5 Parameters and simulation accuracies of optimum regional species-specific models

Species	Number of observation	Optimum model	T_b (°C)	F^* (°C)	P^* (mm)	RMSE (days)
L. chinensis	123	$M_{t\text{-}p1}$	0.0	119.7	2.5	6.8
S. baicalensis	43	M_t	0.2	129.4	–	5.0
S. krylovii	68	$M_{t\text{-}p2}$	0.3	106.8	2.6	9.2

green-up data for *Stipa baicalensis* and *Stipa krylovii* at external stations are relatively small, the precision of the spatial validation was evaluated based on the mixed sample of green-up data for the two species at Stipa. Results show that the observed green-up dates of *Leymus chinensis* and *Stipa baicalensis*/*Stipa krylovii* correlate significantly positive with the predicted green-up dates of *Leymus chinensis* and *Stipa baicalensis*/*Stipa krylovii*, and the RMSEs are 9.8 and 10.4 days, respectively (Fig. 6.6). The RMSEs of the spatial validation are 3.0 days larger than the RMSE of the regional modeling for *Leymus chinensis*, and 3.3 days larger than the average RMSE of the regional modeling for *Stipa baicalensis* and *Stipa krylovii*, respectively (Table 6.5).

6.3.6 Spatiotemporal Patterns of Green-up Dates

For reconstructing spatial patterns of green-up dates of the three grass species across the Inner Mongolian Grassland, daily mean air temperature and daily precipitation data at 8 km × 8 km grids from 1983 to 2009 were substituted into the

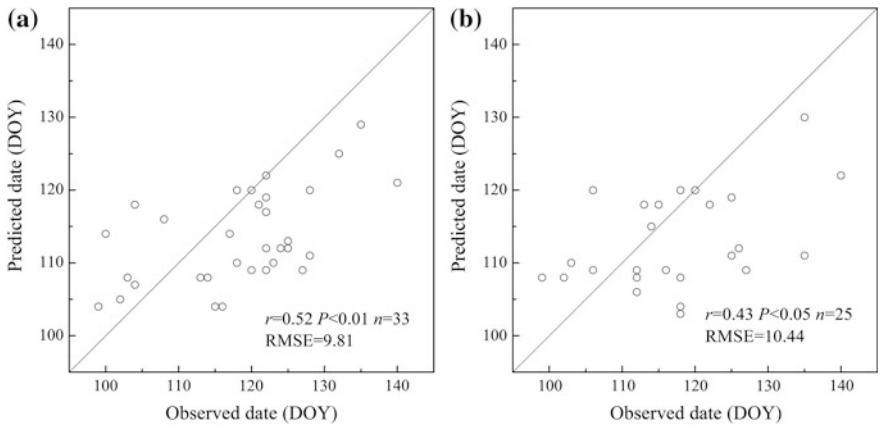

Fig. 6.6 Comparison between observed and predicted green-up dates for **a** *Leymus chinensis* and **b** *Stipa baicalensis*/*Stipa krylovii* at external stations during 2005–2009

three regional models. Because the regional models of *Stipa baicalensis* and *Stipa krylovii* were created within meadow steppe areas and typical steppe areas, respectively, time series of gridded green-up dates for *Stipa baicalensis* within meadow steppe areas and *Stipa krylovii* within typical steppe areas were reconstructed separately, and then merged together for illustrating spatial patterns of green-up dates and their linear trends during 1983–2009 for the two grass species at Stipa. Generally speaking, the spatial pattern of mean green-up dates for *Leymus chinensis* is similar to that for *Stipa baicalensis*/*Stipa krylovii*. Green-up dates represented a spatial progression from southwest and southeast to north in the southern part and from west to east in the northern part of the Inner Mongolian Grassland, which is aligned approximately along the thermal and moisture gradient. The spatial differences in mean green-up dates for *Leymus chinensis* and *Stipa baicalensis*/*Stipa krylovii* were between 91 DOY (1 April) and 142 DOY (22 May) and between 89 DOY (30 March) and 143 DOY (23 May), respectively (Fig. 6.7).

With regard to spatial patterns of green-up date linear trends, a significant advancement in *Leymus chinensis* green-up dates was detected at 71.4 % of all grids during 1983–2009, and trend values are between 2.2 and 6.0 days per decades. The largest advancing trends appear in southwestern parts of the Inner Mongolian Grassland. Nonsignificant trends are mainly located in the central and eastern parts of the Inner Mongolian Grassland (Fig. 6.8a). By contrast, a significant advancement in green-up dates of *Stipa baicalensis*/*Stipa krylovii* was only found at 40.3 % of all grids, and trend values range from 2.3 and 6.2 days per decades, which are mainly distributed in the northeastern and southwestern parts of the Inner Mongolian Grassland (Fig. 6.8b).

At regional scales, green-up dates of *Leymus chinensis*, *Stipa baicalensis* and *Stipa krylovii* have significantly advanced at rates of 2.9 days per decade across the Inner Mongolian Grassland, 3.0 days per decade in meadow steppe areas, and 2.2 days per decade in typical steppe areas over 1983–2009, respectively (Fig. 6.9).

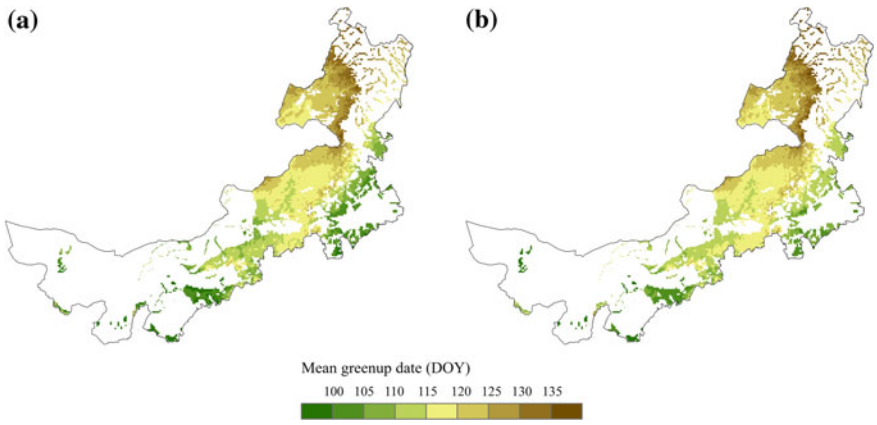

Fig. 6.7 Reconstructed spatial patterns of mean green-up dates for **a** *Leymus chinensis* and **b** *Stipa baicalensis*/*Stipa krylovii* in the Inner Mongolian Grassland during 1983–2009

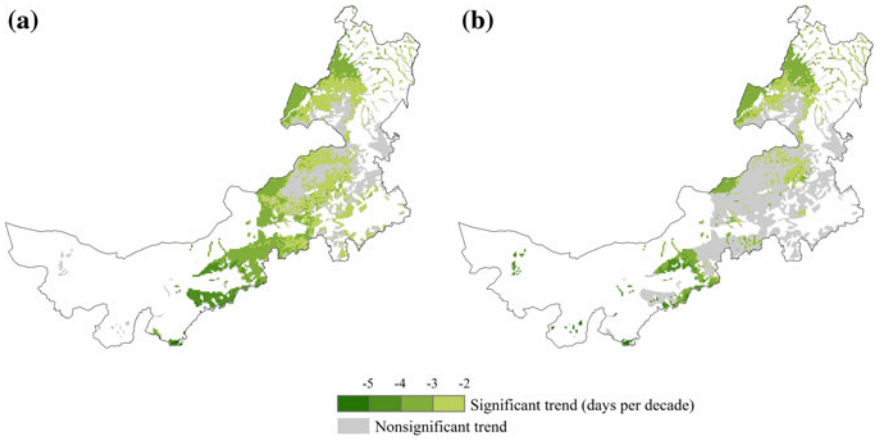

Fig. 6.8 Reconstructed spatial patterns of linear trends of green-up dates for **a** *Leymus chinensis* and **b** *Stipa baicalensis*/*Stipa krylovii* in the Inner Mongolian Grassland during 1983–2009

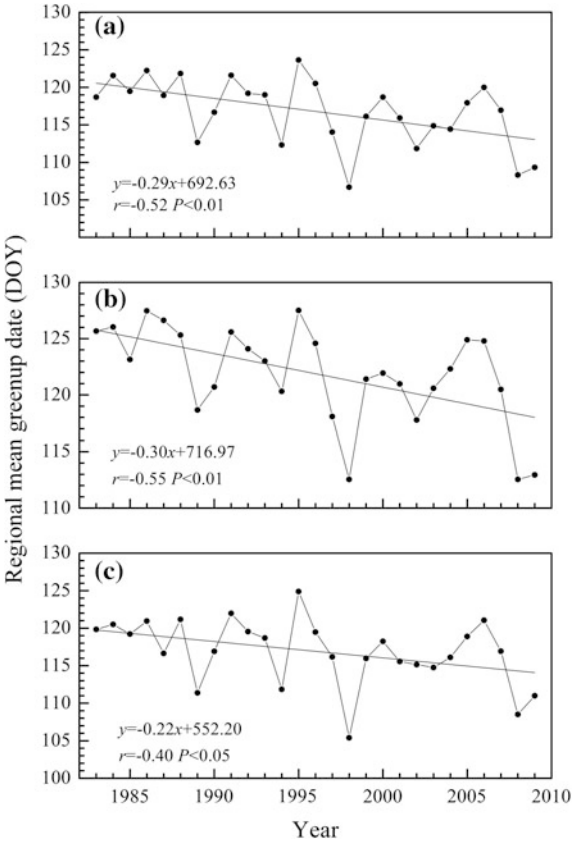

Fig. 6.9 Reconstructed linear trends of green-up dates for **a** *Leymus chinensis* over the Inner Mongolian Grassland **b** *Stipa baicalensis* in meadow steppe areas, and **c** *Stipa krylovii* in typical steppe areas during 1983–2009

References

Akaike H (1973) Information theory and an extension of the maximum likelihood principle. In: Petrov BN, Csaki F (eds) Proceedings of the second international symposium on information theory. Akademiai Kiado, Budapest, pp 267–281

Cannell MGR, Smith RI (1983) Thermal time, chill days and prediction of budburst in *Picea sitchensis*. J Appl Ecol 20:951–963

Chen XQ (2009) Phenological obseration in China. In: Hudson IL, Keatley MR (eds) Phenological research: Methods for environmental and climate change analysis. Springer, Dordrecht, pp 35–38

Chen XQ, Zhou M, Zheng T, Zhang RJ (2008) Examining seasonal variations of *Leymus chinensis* photosynthetic rates in the Hulunbeier Grassland: a case study of a grassland meteorological experiment station in Ewenke (in Chinese with English Abstract). Acta Ecol Sinica 28:2003–2012

Chen XQ, Li J, Xu L, Liu L, Ding D (2014) Modeling greenup date of dominant grass species in the Inner Mongolian Grassland using air temperature and precipitation data. Int J Biometeorol 58:463–471

China Meteorological Administration (1978) Atlas of the climate of China (in Chinese). Sinomaps Press, Beijing

China Meteorological Administration (1993) Observation criterion of agricultural meteorology (in Chinese). China Meteorological Press, Beijing

Chuine I (2000) A unified model for budburst of trees. J Theoret Biol 207:337–347

Chuine I, Cour P, Rousseau DD (1998) Fitting models predicting dates of flowering of temperate-zone trees using simulated annealing. Plant, Cell Environ 21:455–466

Chuine I, Cour P, Rousseau DD (1999) Selecting models to predict the timing of flowering of temperate trees: implications for tree phenology modelling. Plant, Cell Environ 22:1–13

Chuine I, Cambon G, Comtois P (2000) Scaling phenology from the local to the regional level: advances from species-specific phenological models. Global Change Biol 6:943–952

Chuine I, Kramer K, Hänninen H (2003) Plant development models. In: Schwartz MD (ed) Phenology: An integrative environmental science. Kluwer Academic Publishers, Dordrecht, pp 217–235

Cleland EE, Chiariello NR, Loarie SR, Mooney HA, Field CB (2006) Diverse responses of phenology to global changes in a grassland ecosystem. Proc Natl Acad Sci USA 103:13740–13744

Crimmins TM, Crimmins MA, Bertelsen CD (2010) Complex responses to climate drivers in onset of spring flowering across a semi-arid elevation gradient. J Ecol 98:1042–1051

Crimmins TM, Crimmins MA, Bertelsen CD (2011) Onset of summer flowering in a 'SkyIsland' is driven by monsoon moisture. New Phytol 191:468–479

Delpierre N, Dufrêne E, Soudani K, Ulrich E, Cecchini S, Boé J, François C (2009) Modelling interannual and spatial variability of leaf senescence for three deciduous tree species in France. Agric For Meteorol 149:938–948

Editorial Board of the Inner Mongolian Grassland (1991) The Inner Mongolian Grassland (in Chinese). Renmin Press of Inner Mongolia, Huhehot

Fu YH, Campioli M, Van Oijen M, Deckmyn G, Janssens IA (2012) Bayesian comparison of six different temperature-based budburst models for four temperate tree species. Ecol Modelling 230:92–100

García-Mozo H, Chuine I, Aira MJ, Belmonte J, Bermejo D, Díaz de la Guardia C, Elvira B, Gutiérrez M, Rodríguez-Rajo J, Ruiz L, Trigo MM, Tormo R, Valencia R, Galán C (2008) Regional phenological models for forecasting the start and peak of the *Quercus* pollen season in Spain. Agric For Meteorol 148:372–380

Hall DO, Scurlock JMO, Ojima DS, Parton WJ, Wigley TML, Schimel D (2000) Grasslands and the global carbon cycle: modeling the effects of climate change. In: Wigley TML, Schimel DS (eds) The carbon cycle. Cambridge University Press, Cambridge, pp 102–114

Hänninen H (1990) Modelling bud dormancy release in trees from cool and temperate regions. Acta For Fenn 213:1–47

Hunter AF, Lechowicz MJ (1992) Predicting the timing of budburst in temperate trees. J Appl Ecol 29:597–604

Hutchinson MF (2002) Anusplin Version 4.2 User Guide. Centre for Resource and environmental studies. The Australian National University, Canberra

Jentsch A, Kreyling J, Boettcher-Treschkow J, Beierkuhnlein C (2009) Beyond gradual warming: extreme weather events alter flower phenology of European grassland and heath species. Global Change Biol 15:837–849

Kramer K (1994a) A modeling analysis of the effects of climatic warming on the probability of spring frost damage to tree species in the Netherlands and Germany. Plant, Cell Environ 17:367–377

Kramer K (1994b) Selecting a model to predict the onset of growth of *Fagus sylvatica*. J Appl Ecol 31:172–181

Landsberg JJ (1974) Apple fruit bud development and growth; analysis and an empirical model. Ann Bot 38:1013–1023

Lesica P, Kittelson PM (2010) Precipitation and temperature are associated with advanced flowering phenology in a semi-arid grassland. J Arid Environ 74:1013–1017

Linkosalo T, Lappalainen HK, Hari P (2008) A comparison of phenological models of leaf bud burst and flowering of boreal trees using independent observations. Tree Physiol 28:1873–1882

Morin X, Lechowicz MJ, Augspurger C, O'Keefe J, Viner D, Chuine I (2009) Leaf phenology in 22 North American tree species during the 21st century. Global Change Biol 15:961–975

Murray MB, Cannell MGR, Smith RI (1989) Date of budburst of fifteen tree species in Britain following climatic warming. J Appl Ecol 26:693–700

Nash JE, Sutcliffe JV (1970) River flow forecasting through conceptual models part I—a discussion of principles. J Hydrol 10:282–290

Sherry RA, Zhou XH, Gu SL, Arnone JA, Schimel DS, Verburg PS, Wallace LL, Luo YQ (2007) Divergence of reproductive phenology under climate warming. Proc Natl Acad Sci USA 104:198–202

Shinoda M, Ito S, Nachinshonhor GU, Erdenetsetseg D (2007) Phenology of Mongolian grasslands and moisture conditions. J Meteorol Soc Jap 85:359–367

Study Group of Animal Husbandry Climate Regionalization for China's Pastoral Areas (1988) Animal husbandry climate for China's pastoral areas (in Chinese). China Meteorological Press, Beijing

Xu L, Chen XQ (2013) Regional unified model-based leaf unfolding prediction from 1960 to 2009 across northern China. Global Change Biol 19:1275–1284